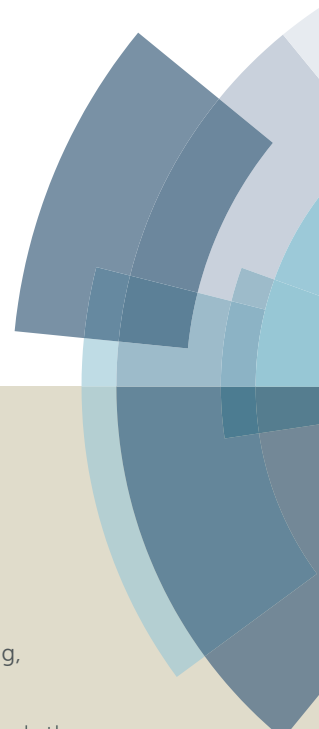
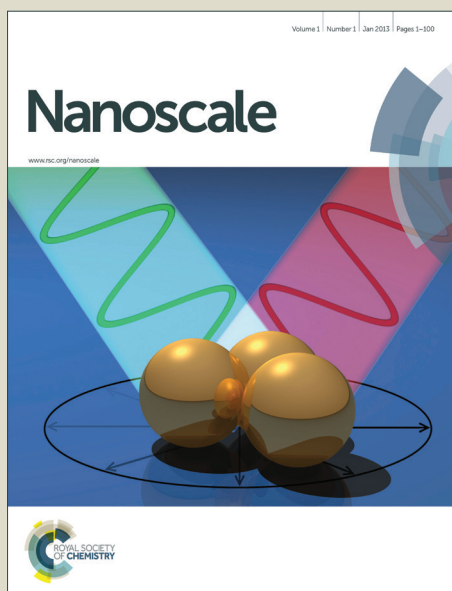


Nanoscale

Accepted Manuscript



This article can be cited before page numbers have been issued, to do this please use: H. Tang, C. Yang, Z. Lin, Q. Yang, F. Kang and C. P. Wong, *Nanoscale*, 2015, DOI: 10.1039/C5NR00465A.



This is an *Accepted Manuscript*, which has been through the Royal Society of Chemistry peer review process and has been accepted for publication.

Accepted Manuscripts are published online shortly after acceptance, before technical editing, formatting and proof reading. Using this free service, authors can make their results available to the community, in citable form, before we publish the edited article. We will replace this *Accepted Manuscript* with the edited and formatted *Advance Article* as soon as it is available.

You can find more information about *Accepted Manuscripts* in the [Information for Authors](#).

Please note that technical editing may introduce minor changes to the text and/or graphics, which may alter content. The journal's standard [Terms & Conditions](#) and the [Ethical guidelines](#) still apply. In no event shall the Royal Society of Chemistry be held responsible for any errors or omissions in this *Accepted Manuscript* or any consequences arising from the use of any information it contains.

ARTICLE

ARTICLE

Journal Name

Electrospray-deposition of graphene electrode: a simple technique to build high-performance supercapacitors

Cite this: DOI: 10.1039/x0xx00000x

Huaichao Tang,^a Cheng Yang,^{*a} Ziyin Lin,^b Quanhong Yang,^a Feiyu Kang,^{a,c} Ching Ping Wong^{b,d}Received 00th January 2015,
Accepted 00th January 2015

DOI: 10.1039/x0xx00000x

www.rsc.org/

Here we report an electrostatic spray deposition method to prepare three-dimensional porous graphene electrode for supercapacitor applications. The symmetric supercapacitor exhibits excellent specific capacitance (366 Fg^{-1} at 1 Ag^{-1} in 6 M KOH) and long cycle life (108% capacitance retention up to 40,000 cycles). Moreover, the energy densities of the organic and aqueous electrolyte based supercapacitors reach 22.9 and 8.1 Wh/kg when the power densities are 119.2 and 15.4 kW/kg, respectively. As compared with the ever-reported graphene based supercapacitors, the improved properties could be attributed to the excellent three-dimensional open porous electrode structure, which is favorable for the ion diffusion and electron transport. In addition, this method provides a simple electrode-fabrication route without the involvement of conducting additives and binders. It may find vast applications in thin and miniaturized energy storage scenarios.

Introduction

Owing to its excellent electrical conductivity, superior specific surface area, extraordinary chemical stability and mechanical strength, graphene has attracted significant interests in the fields of energy storage application, such as supercapacitors and lithium ion batteries.¹⁻⁴ Yet currently, there are still a few issues to be addressed before they find broader applications; one of the biggest issues is its tendency to irreversibly aggregate due to the strong van der Waals attraction, especially when graphene experiences compressions during the electrode fabrication process,⁵⁻⁷ which results in the loss of accessible surface area.⁸ Additionally, conventional casting and rolling processes for graphene electrodes often induce lamellar arrangement of the two-dimensional (2D) graphene nanosheets along the lateral direction of the current collector, which hinder the ion mobility in vertical direction.^{9,10} Besides, electrochemically inactive additives e.g. polymer binders are often required for the graphene-based active materials, which not only increase the complexity of electrode preparations but also reduce the specific capacitive performance.¹¹⁻¹³

To address the above challenges, a few attempts have been made recently in the fabrication of graphene-based electrodes, e.g. activation of graphene,¹⁴ doping of graphene,^{15,16} hybridization of graphene using physical/chemical assemblies on metal oxides, combining conducting polymers or carbon nanotube (CNT) connectors,¹⁷⁻¹⁹ rendering mesoporous graphene nanofibers, gelation of graphene, and crumpling of graphene etc.²⁰⁻²² Among the above attempts, crumpling graphene method has attracted much attention for supercapacitor studies.²²⁻²⁴ Analogous to the crumpled paper, the crumpled graphene can maintain the large surface area, three

dimensional (3-D) structure and excellent compression-resistant properties,^{23,24} which facilitates the multi-dimensional electron transport and rapid ion diffusions between electrodes. Huang and co-workers for the first time fabricated crumpled graphene oxide (GO) balls by nebulizing the GO suspension in a carrying gas; the subsequently reduced crumpled GO balls were used as active material by the conventional electrode casting method, and the electrode capacitance reached 150 Fg^{-1} .²⁴ Even though the crumpling method shows great promise in improving the volumetric capacitive capability, it still involves conventional casting processing method, which becomes incompatible with the ever growing micro-supercapacitor device technology that is featured with smaller and thinner electrode feature size and higher specific capacitance of the electrode materials.

Here we first report a simple electrostatic spray deposition (ESD) fabrication process for the highly uniform 3-D open porous crumpled reduced GO (C-rGO) electrode. ESD technique has been widely studied for decades in the surface coating industry,^{25,26} which can effectively improve the uniformity of particles/droplets in the sprayed area. Recently, Beidaghi and coworkers for the first time attempted to utilize ESD to deposit graphene films, yet only a thin layer of graphene nanoplatelets was obtained.²⁶ Despite the numerous advantages for the ESD method, the limited knowledge about how to construct 3-D open porous graphene nanostructure greatly hinders the application of ESD for the fabrication of high performance electrodes. In this work, we demonstrate an improved ESD method to construct the crumpled graphene electrodes. A unique characteristic here is the involvement of an electric stove,

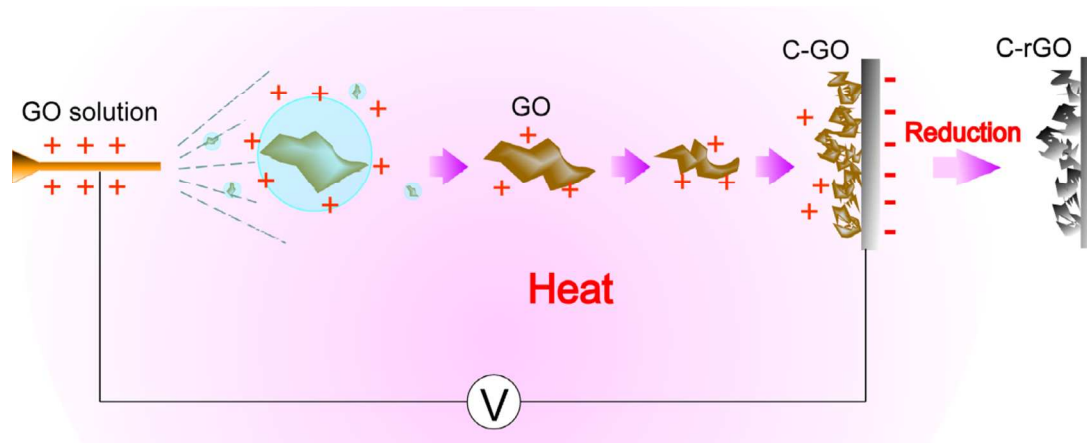


Fig. 1 Schematic illustration of the process for fabricating C-GO and C-rGO.

which is placed at the bottom of the spread region to render a high-temperature zone. When the aerosolized GO particles fly through such a heated region, the solvent in GO droplets evaporates rapidly and thus effectively trigger the crumpling process.²⁷ In this way, C-GO are deposited homogeneously on the opposite stainless steel collector, and the thickness of this layer can be adjusted conveniently by tuning the experimental conditions (such as deposition time, voltage, surface tension of the suspension and pumping rate etc.). Subsequently, this 3-D porous C-GO film can be reduced by a hydrazine-thermal reduction treatment process and directly used as supercapacitor electrodes without adding any additive. Using such a simple method, excellent specific capacitance (366 Fg^{-1}) can be obtained for the symmetrical supercapacitor device at a current density 1 Ag^{-1} in 6 M KOH aqueous electrolyte, which is more than triple of the capacitance of the naturally dried uncrumpled reduced graphene oxides (N-rGO, 92 Fg^{-1} , see Supporting Information for details). Moreover, the C-rGO based supercapacitor exhibited excellent cycling stability and rate performance. The specific capacitance and energy density of our supercapacitors with aqueous electrolyte list one of the highest values among the recently reported graphene based supercapacitors.²⁸⁻³¹

Methodology

Fabrication of the graphene oxide (GO) resolution and crumpled GO (C-GO):

GO was first prepared from graphite powder by a modified Hummers method.³² It was then subjected to strong sonication (200W, JY92-N, a high-energy bench mounted ultrasonic disintegrator) in deionized water for 2 h to obtain a homogeneous GO hydrosol with a concentration of 2 mg mL^{-1} .

In a typical sample fabrication process, 2 mg mL^{-1} of aqueous solution was added to absolute ethyl alcohol in a range of ratio about 1:3-1:10 and then sonicated for 30 min with a sonicator (300W, JY92-N, a high-energy bench mounted ultrasonic disintegrator). Subsequently, the GO suspension was fed into a stainless steel nozzle (internal diameter 0.84mm) through a syringe pump at a feeding rate of 0.15 to 0.30 mL/min, and a voltage of 30-35 kV. The distance between the nozzle and the stainless steel substrate was set to 25 cm. An electric furnace is placed at bottom of the region between the nozzle and the collector to accelerate the evaporation of solvent. The deposition times and the feeding rate can be adjusted to obtain desirable thicknesses and homogeneity of the film. For the

non-crumpled GO (N-GO) control sample, the same mixture solution was doctor-bladed on the stainless steel plate and this plate was dried by furnace in $50 \text{ }^\circ\text{C}$ for 24h (0.05 mg/cm^2). C-rGO electrodes with higher thickness (e.g. five times thicker) were obtained by repeating the deposition and reduction process.

Fabrication of the crumpled reduced GO (C-rGO) and N-rGO:

In order to maintain the 3-D macroporous structure during the reduction process, both C-GO and N-rGO samples were reduced in the hydrazine hydrate vapor at $85 \text{ }^\circ\text{C}$ for 10 h to release most of the oxygen groups. After that, both of them were characterized in dry conditions. By spraying for one cycle, the surface density is 0.07 mg/cm^2 . Multiplying the deposition-reduction cycles can effectively improve the areal active mass loadings.

Material characterization:

The morphology and microstructure of the C-GO and C-rGO were characterized by the field emission scanning electron microscopy (FE-SEM, HITACH S4800, Japan) and transmission electron microscopy (TEM, JEOL-2100F). Raman spectra were recorded on a Jobin-Y von Horbia 800 using a 632.8 nm laser. Fourier transform infrared (FTIR) spectra were recorded on a FTIR system (Nicolet iS10, USA) equipped with a Smart Attenuated Total Reflectance (Smart ATR) appendix. The Raman spectroscopy measurements were measured using a HOIBA HR800 Raman system with an excitation wavelength 532 nm. The X-ray photoelectron spectroscopy (XPS) measurements (ESCALAB 250Xi) of the materials were performed to analyze the surface species and their chemical states on an Axis Ultra photoelectron spectrometer using an Al K α (1486.7eV) X-ray source. Deconvolution and spectral line fitting were carried out using XPS Peak 4.0.

Electrochemical characterizations:

Two slices of C-rGO and N-rGO ($1.0 \times 0.5 \text{ cm}^2$) were assembled as the electrodes directly without grinding and compressing to symmetric cells with 6.0 M KOH solution in atmosphere, respectively. No binder or conductive additive was used. The C-rGO electrodes were assembled with EMIMBF₄ in a glove box in Ar atmosphere. The surface density by mass of C-rGO was calculated by the weight difference of the same electrode before and after stripping off C-rGO.

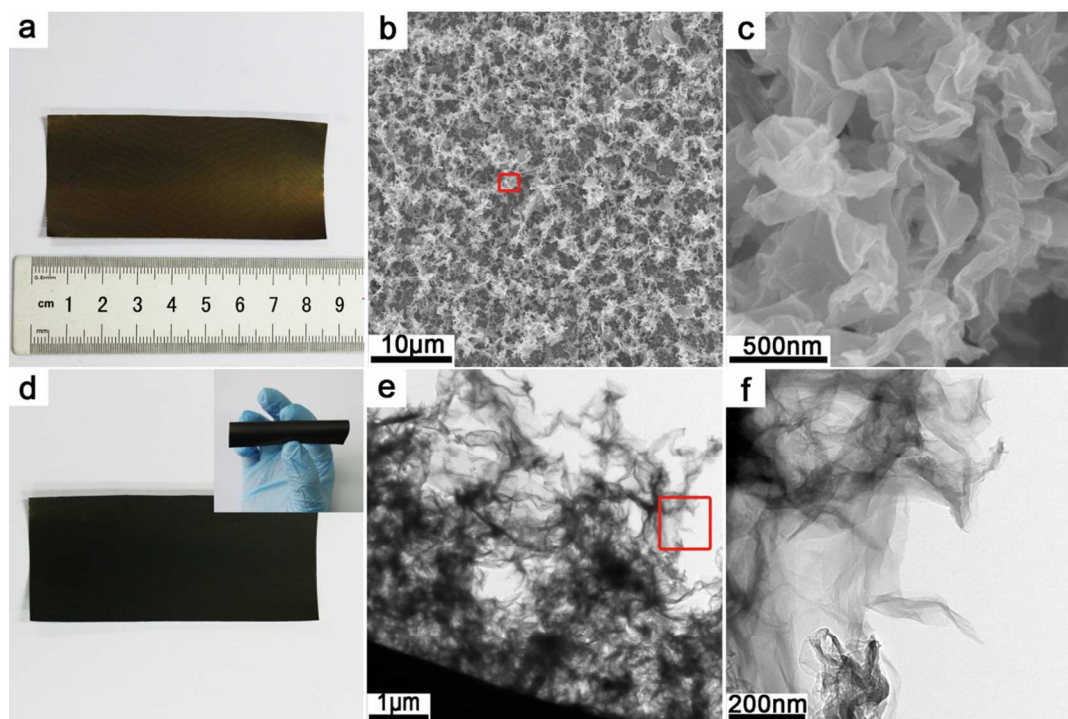


Fig. 2 (a) Photographic image of the as-prepared C-GO. (b) SEM image of the as-prepared C-GO. (c) magnified SEM image of the outlined region in (b). (d) Photographic image of the C-rGO. (e) TEM image of the cross section C-rGO sample. (f) HR-TEM images of the outlined area in (e).

The electrochemical properties of the as-prepared electrodes were evaluated on an electrochemical station (VMP3, Bio-Logic, France). Cyclic voltammetry (CV) and galvanic charge/discharge (GCD) measurements of all the cells were performed in the operating potential range from 0 to 0.8V (N-rGO and C-rGO, respectively) with aqueous electrolyte and 0 to 2.5V with organic electrolyte. The cycle life tests were performed by the GCD measurements. Electrochemical impedance spectroscopy (EIS) was performed over a frequency range from 100 kHz and 0.1 Hz at an amplitude of 5 mV. For the self-discharge test, the device was first charged to 0.8 V and kept at 0.8 V for 30 min, and then the open potential of the device was recorded as a function of time.

Results and discussions

The preparation process of C-rGO is illustrated in Fig. 1. Firstly, the GO nanosheets prepared by Hummers method is dispersed in a solution mixture of deionized water and absolute ethanol (1:3-1:10).³² Then this suspension is pumped out through a stainless steel nozzle with a steady speed (ranging from 0.15 to 0.30 mL/min), and subsequently aerosolized at the tip of the nozzle by applying high electric potential (25-40 kV). The distance between the nozzle and the stainless steel collector can be adjusted from 25 to 50 cm (here we chose 25 cm). The crumpling process can be accelerated by heating the spraying zone (about 100 °C, confirmed by thermal couple measurement in this region) using an electric furnace in open air. During the aerosolizing process, the solvent in the tiny droplets can be rapidly evaporated. The evaporation of the remnant solvent sandwiched between two hydrophilic GO surfaces can exert a capillary force on the GO nanosheets, which can induce the GO nanosheets to form ridges until the GO nanosheets transform into the

C-GO.^{25,28} Subsequently, the dried C-GO landed on the stainless steel collector substrate is reduced to C-rGO by exposure to the hydrazine hydrate vapor at 85°C for 10 hours.

As shown in Fig. 2a and Fig. 2d, the as-prepared C-GO layer is in brown color, while the C-rGO is totally black. This distinctive color change indicates the reduction of C-GO. It is noteworthy that the crumpling process can be tuned by adjusting the deposition parameters, such as flow rate, temperature, the applied voltage, geometric parameters of the instrument setup and composition of the GO solution etc. Additionally, the thickness of the deposited film can be controlled by repeating the spraying and reducing steps. (See Supporting Information for details.) As shown in the inset of Fig. 2d, the stainless steel film carrying C-rGO can be bent repeatedly without losing graphene powder, suggesting adequate binding force (van der Waals force) between the C-rGO and the stainless steel substrate. Scanning electron microscopy (SEM) analysis of C-rGO reveals that C-rGO has a disordered microstructure and there are abundant wrinkled structures (Fig. 2b and 2c). The C-rGO pieces are randomly associated with each other, which are quite different from those of the N-rGO films dried naturally and the previous report (See Supporting Information Fig. S1a and S1b).²⁶

The high resolution transmission electron microscopy (HR-TEM) images of the C-rGO cross section sample are shown in Fig. 2e-f, which show the microstructural characteristic of C-rGO. There were abundant wrinkles and ripples of the open porous structure on both the surface of C-GO and C-rGO, showing a hierarchical 3-D porous structure (Fig. S2 a-c). Furthermore, based on the TEM observations of the C-rGO sheets (Fig. S2d), these C-rGO are the few-layer ones, which are loosely associated with each other, forming a uniform layer.

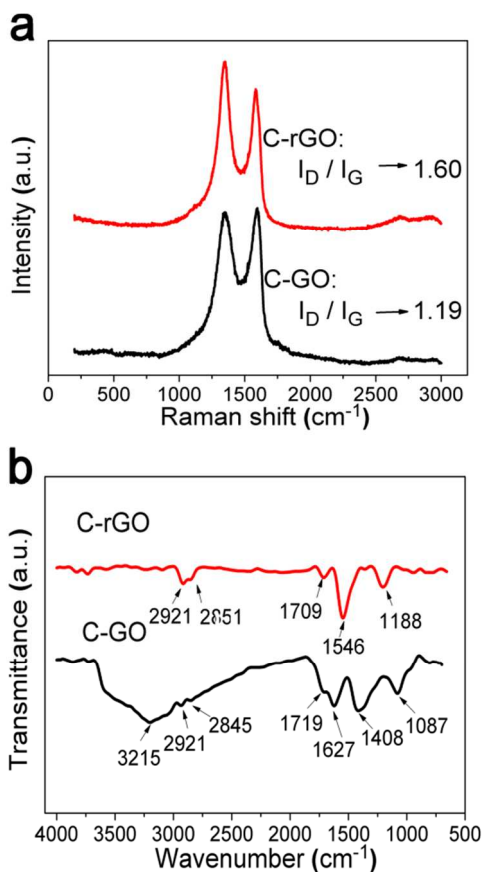


Fig. 3 (a) Raman spectra of C-GO and C-rGO. (b) FTIR spectra of C-GO and C-rGO.

The structural information of both C-GO and C-rGO can be investigated by Raman and Fourier transform infrared spectroscopy (FTIR) (Fig. 3a and 3b). In the Raman spectra (Fig. 3a), D band and G band appear at 1363 and 1596 cm^{-1} for C-GO, whereas they are shifted to 1341 cm^{-1} and 1583 cm^{-1} for C-rGO, respectively. This downshifted G band position after reduction matched well with that of pristine graphene.³³ Meanwhile, as an indicator of the degree of disorder and average size of the sp^2 domains,³⁴ the values of I_D/I_G increased from 1.19 to 1.60 when C-GO was converted to C-rGO.

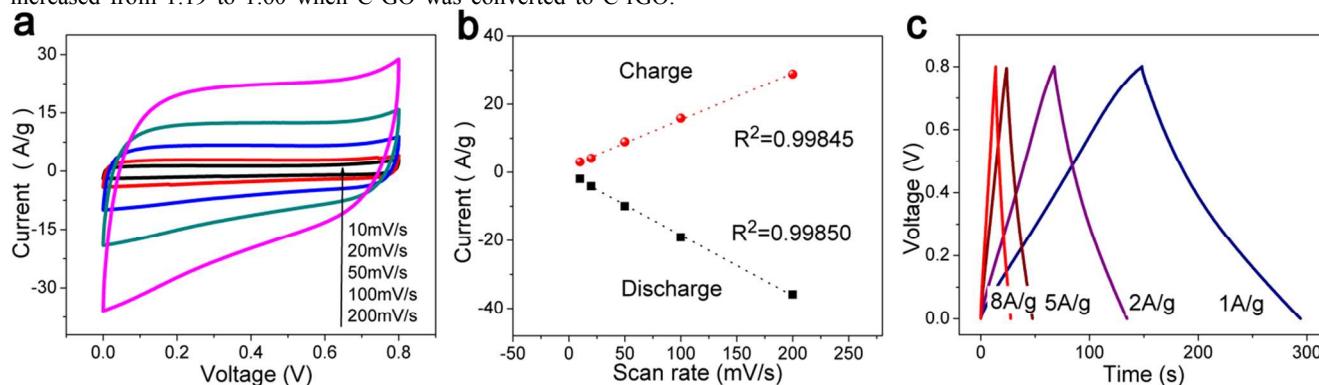


Fig. 4 (a) The cyclic voltammetry (CV) curves of C-rGO in a two-electrode system at different scan rate and current densities in 6M KOH. (b) The charge-discharge current vs. scan rate curve (extracted from the CV curves scanning between 0 to 0.8V). (c) The galvanostatic charge-discharge (GCD) curves of the same sample.

Furthermore, the significant changes in the FTIR spectra (Fig. 3b) confirmed the reduction of C-GO on the stainless steel film. The intensities of those adsorption peaks corresponding to the oxygen-containing functional groups (3215 cm^{-1} due to O-H stretching vibration, 1408 cm^{-1} due to carboxyl C-O stretching vibration, and 1087 cm^{-1} due to alkoxy C-O stretching vibration) decreased substantially,³⁵ which suggested that most oxygen-containing functional groups of C-GO were eliminated, which inferred an improved electrical conductance.³⁶ Additionally, X-ray photoelectron spectroscopy (XPS) analysis suggested that the C/O ratio of C-GO and C-rGO increased from 0.56 to 1.21, indicating the partial reduction of C-GO (Fig. S3). Besides, an N_{1s} peak can be observed for that of C-rGO, which is due to the involvement of hydrazine hydrate in the reducing process. The incorporation of nitrogen atoms may possibly further improve the electrochemical performance of C-rGO electrode.³⁷

In view of the stable 3-D open porous structure, this C-rGO film can be directly used as the electrode for fabricating a symmetrical supercapacitor (electrode size: $1.0 \times 0.5 \text{ cm}^2$). Both aqueous (6.0 M KOH) and organic (1-ethyl-3-methylimidazolium tetrafluoroborate concentration and solvent, EMIMBF₄) electrolytes were used. For comparison, a control sample of non-crumpled rGO (N-rGO) electrode was used and fabricated by conventional casting method. As shown in Fig. 4a, the cyclic voltammetry (CV) spectra of the C-rGO based symmetric supercapacitors with 6.0 M KOH electrolyte showed quasi-rectangular shapes, and the shapes of the CV curves were well maintained even the scan rate increased from 10 to 200 mV s^{-1} , revealing excellent rate capability. Fig. 4b shows the dependence of the capacitive current (extracted from the CV profiles at 0 and 0.8 V for the charge/discharge curves, respectively) at the corresponding scan rates. These charge/discharge current densities of the C-rGO supercapacitor are almost linear-proportional and the linear relationships conform to $R^2 = 0.99845$ and 0.99850 for the charge and discharge curves respectively. The galvanostatic charge/discharge (GCD) curves of the C-rGO supercapacitor at various current densities of 1, 2, 5 and 8 A g^{-1} were triangular (Fig. 4c), confirming the major electrical double layer type charge storage mechanism.³⁸ Furthermore, there was a small voltage drop (such as 0.005V at 1 A g^{-1}) at the starting point of the discharge curve of GCD, also indicating that the C-rGO supercapacitor has small solution resistance and internal charge transfer resistance. (The equivalent series resistance is about 0.18 Ω at 1 A g^{-1} .)

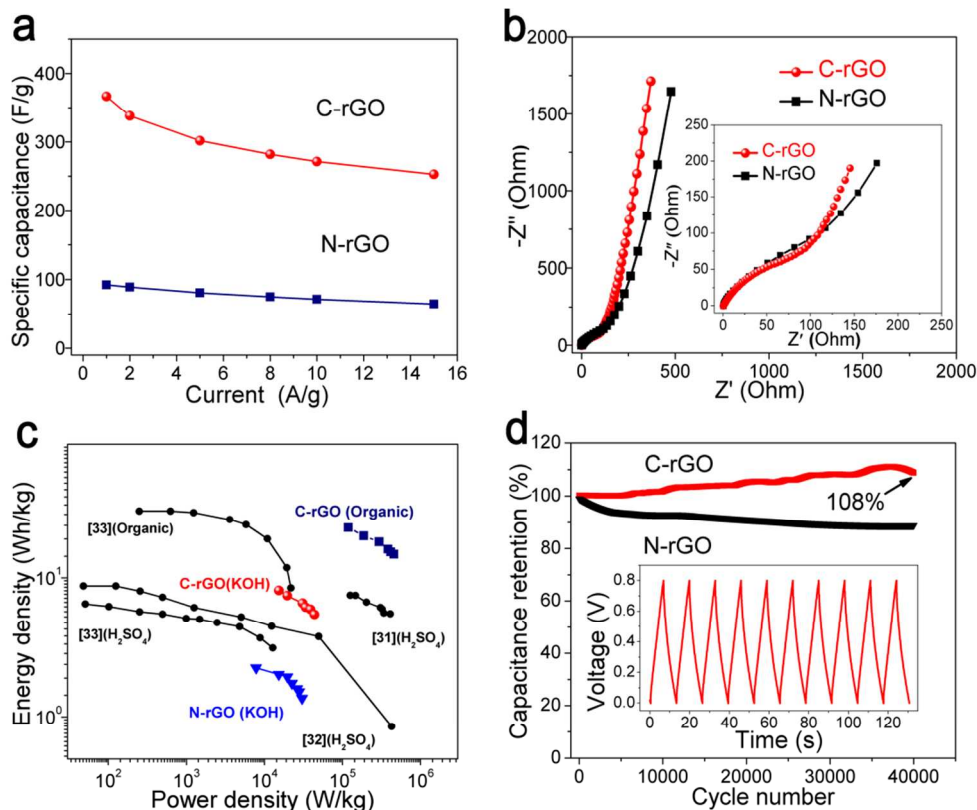


Fig. 5 (a) Specific capacitance of C-rGO and N-rGO with aqueous electrolyte as a function of the current densities. (b) Nyquist plots of the C-rGO and N-rGO; the inset is the magnified high-frequency region. (c) The Ragone plot of C-rGO and N-rGO based symmetric supercapacitor and some other recently reported results. (d) The capacitance retention of C-rGO and N-rGO as a function of cycling number with the inset of a GCD curve of C-rGO at 15 Ag⁻¹.

More importantly, the specific capacitance of C-rGO with 6 M KOH electrolyte was recorded up to 366 Fg⁻¹ at 1 Ag⁻¹ (Fig. 5a, more measurement details in supporting information), which was much larger than that of N-rGO (92 Fg⁻¹ at 1 Ag⁻¹). Notably, even at the fast discharge rate of 15 Ag⁻¹, a high specific capacitance of 253 Fg⁻¹ was still maintained, which was three times higher than that of N-rGO (65 Fg⁻¹ at 15 Ag⁻¹). It is noteworthy that the capacitance observed in C-rGO is even higher than those of graphene supercapacitors reported previously.^{28-31,39} In addition, self-discharge performance of the C-rGO based supercapacitor (Fig. S4) suggested that even after 5 hours, more than 60% voltage value was maintained, implying that the 3-D freestanding structure of C-rGO was favorable for the charge redistribution process.¹⁸ On the basis of these results, we further investigated the electrochemical performance of C-rGO films by elongating and repeating the deposition process (Fig. S5 and S6). It shows that the areal capacitance of C-rGO is linearly proportional to the deposition time, indicating the thickness of C-rGO on the stainless steel film can be adjusted accurately in the experiment.

Cycling stability is another crucial factor for evaluating the supercapacitors. The C-rGO aqueous supercapacitor showed excellent electrochemical stability and high reversibility, which were confirmed by the GCD cycling test at a current density of 15 Ag⁻¹ up to 40,000 cycles. As shown in Fig. 5d, the specific capacitance retention of N-rGO supercapacitor continuously decreased within the 40,000 cycles. In contrast, the capacitances of C-rGO did not degrade but slightly increased, for example, after 20,000 cycles, the increase of capacitance was less than 5%; after 40,000 cycles, the

capacitive increased to 108% of the initial capacitance, showing good potential for fabricating high performance energy storage devices. The increased capacitance of C-rGO may be related to the increased surface area which is accessible to the electrolytes during the long time cycling, which is referred as “electro-activation”.^{40,41} It was suggested that the electrolyte ions intercalate into the space of the graphene sheets and lead to a larger spacing between the layers during the charge/discharge process. Therefore, it can increase the accessibility of ions to the surface of graphene, which is important for the electric double-layer capacitance.

According to the electrochemical impedance spectroscopy (EIS) (Nyquist plots) from 0.1 Hz to 100 kHz at an amplitude of 5 mV, the C-rGO supercapacitor exhibits excellent capacitive behavior and low internal resistance (Fig. 5b). The sharp slope of that of C-rGO was more vertical than that of N-rGO in the low-frequency region, indicating better electrochemical performance of C-rGO, with an improved ion transport in the electrodes.⁴² Moreover, the semi-circle in the impedance curve (Fig. 5c inset) for C-rGO was found to be smaller than that for N-rGO, suggesting a smaller charge-transfer resistance than N-rGO.⁴³

In order to further explore the electrochemical property of C-rGO in a larger electrochemical window, we fabricated the C-rGO supercapacitor with organic electrolyte (EMIMBF₄), which has a higher working voltage of 2.5 V for high energy density (Fig. S7). The CV curve of such an organic supercapacitor exhibited a rectangular shape within a selected range of potential from 0 to 2.5 V (Fig. S7a). The short-cut current was smaller than that of the

aqueous based supercapacitor at the same scan rate (Fig. S7b); the open-circuit potential of organic supercapacitor was more than three times higher than that of an aqueous supercapacitor, which suggested a high energy density. The nearly triangular shape of the charge-discharge curve (Fig. S7c) at current densities of 1, 2, 5 and 8 Ag⁻¹ was similar to the GCD curve of aqueous supercapacitor. Furthermore, the EIS curve had a smaller semi-circle in high frequency region and an almost vertical line in the low frequency region, confirming the fast ion diffusion in the 3-D open porous electrode (see Supporting Information for details).³⁹ As shown in the Ragone plot (Fig. 5c), the highest energy density of organic and aqueous C-rGO supercapacitor were recorded up to 22.9 and 8.1 Wh/kg with a power density of 119.2 and 15.4 kW/kg, respectively, while it was only 2.2 Wh/kg for the N-rGO aqueous supercapacitor with the power density of 7.8 kW/kg. This electrochemical capacitive performance of the C-rGO is excellent among the recently reported ones in comparable testing conditions.²⁸⁻³¹

Concluding Remark and Outlook

In summary, we developed a simple and effective ESD fabrication method to prepare the high quality 3-D open porous C-rGO electrodes. This method shows a series of technical advantages, for example, 1) ESD is a cheap, scalable, and highly reproducible technique; 2) the GO pieces can be sprayed out very homogeneously in open air and form uniform crumpled particles very conveniently; 3) after the hydrazine-thermal treatment, the C-rGO powders have adequate bonding with each other and to the stainless steel substrate (possibly through van der Waals force), which render the deposited film to be used as the electrode without the involvement of any complex assembly step or additive. Although the C-rGO is not perfectly single-layer, the 3-D open porous structure enables excellent Ohmic conductive network and provides highly efficient ion diffusion path, and thus facilitating the migration of charge carriers during the charge/discharge process. Based on the above technical advances, the symmetric C-rGO supercapacitor device exhibited high specific capacitance (366 Fg⁻¹) at a current density of 1 Ag⁻¹ in 6 M KOH aqueous solution and very long cycle life (108% capacitance retention up to 40,000 cycles). The highest energy density of organic electrolyte based C-rGO supercapacitor was up to 22.9 Wh/kg with a power density of 119.2 kW/kg. Taking all above advantages, this technique may become a general path for the preparation of graphene analogues and composite materials with 3-D structure in the near future. We believe that this technology holds a promise for broad applications, such as energy storage and frequency modulation devices, catalyst carriers, air filters and adsorbents, etc.

Acknowledgements

This research is partially funded by the National Natural Science Foundation of China (51202120), the National Key Basic Research (973) Program (2014CB932400), and Shenzhen Government (KQCX20120814155245647 and CYJ20130402145002411).

Notes and references

- a Division of Energy and Environment, Graduate School at Shenzhen, Tsinghua University, Shenzhen 518055, P. R. China;
b School of Materials Science and Engineering, Georgia Institute of Technology, 771 Ferst Dr. Atlanta, GA 30332, U.S.A;
c School of Materials Science and Engineering, Tsinghua University, Beijing 100084, China;

d Department of Electronic Engineering, The Chinese University of Hong Kong, Hong Kong

E-mail: yang.cheng@sz.tsinghua.edu.cn

† Electronic Supplementary Information (ESI) is also included. See DOI: 10.1039/b000000x/

- J. R. Miller, R. A. Outlaw and B. C. Holloway, *Science*, 2010, **329**, 1637-1639.
- M. Hassan, E. Haque, K. R. Reddy, A. I. Minett, J. Chen and V. G. Gomes, *Nanoscale*, 2014, **6**, 11988-11994.
- L. Ji, M. Rao, H. Zheng, L. Zhang, Y. Li, W. Duan, J. Guo, E. J. Cairns and Y. Zhang, *J. Am. Chem. Soc.*, 2011, **133**, 18522-18525.
- W. Lv, D.-M. Tang, Y.-B. He, C.-H. You, Z.-Q. Shi, X.-C. Chen, C.-M. Chen, P.-X. Hou, C. Liu and Q.-H. Yang, *ACS Nano*, 2009, **3**, 3730-3736.
- J. Chang, M. Jin, F. Yao, T. H. Kim, V. T. Le, H. Yue, F. Gunes, B. Li, A. Ghosh, S. Xie and Y. H. Lee, *Adv. Funct. Mater.*, 2013, **23**, 5074-5083.
- Y. He, W. Chen, X. Li, Z. Zhang, J. Fu, C. Zhao and E. Xie, *ACS nano*, 2012, **7**, 174-182.
- G. Huang, C. Hou, Y. Shao, B. Zhu, B. Jia, H. Wang, Q. Zhang and Y. Li, *Nano Energy*, 2015, **12**, 26-32.
- S. H. Aboutalebi, A. T. Chidembo, M. Salari, K. Konstantinov, D. Wexler, H. K. Liu and S. X. Dou, *Energy & Envir. Sci.*, 2011, **4**, 1855-1865.
- J. J. Yoo, K. Balakrishnan, J. Huang, V. Meunier, B. G. Sumpter, A. Srivastava, M. Conway, A. L. Reddy, J. Yu, R. Vajtai and P. M. Ajayan, *Nano Lett.*, 2011, **11**, 1423-1427.
- Z. Bo, W. Zhu, W. Ma, Z. Wen, X. Shuai, J. Chen, J. Yan, Z. Wang, K. Cen and X. Feng, *Adv. Mater.*, 2013, **25**, 5799-5806.
- H. Wang, H. S. Casalongue, Y. Liang and H. Dai, *J. Am. Chem. Soc.*, 2010, **132**, 7472-7477.
- Y. Xu, M. G. Schwab, A. J. Strudwick, I. Hennig, X. Feng, Z. Wu and K. Müllen, *Adv. Energy Mater.*, 2013, **3**, 1035-1040.
- H. Kim, M.-Y. Cho, M.-H. Kim, K.-Y. Park, H. Gwon, Y. Lee, K. C. Roh and K. Kang, *Adv. Energy Mater.*, 2013, **3**, 1500-1506.
- Y. Tao, X. Xie, W. Lv, D. M. Tang, D. Kong, Z. Huang, H. Nishihara, T. Ishii, B. Li, D. Golberg, F. Kang, T. Kyotani and Q. H. Yang, *Sci. Rep.*, 2013, **3**, 2975.
- Z. S. Wu, K. Parvez, A. Winter, H. Vieker, X. Liu, S. Han, A. Turchanin, X. Feng and K. Mullen, *Adv. Mater.*, 2014, **26**, 4552-4558.
- X. Huang, Z. Zeng, Z. Fan, J. Liu and H. Zhang, *Adv. Mater.*, 2012, **24**, 5979-6004.
- Z. Fan, J. Yan, L. Zhi, Q. Zhang, T. Wei, J. Feng, M. Zhang, W. Qian and F. Wei, *Adv. Mater.*, 2010, **22**, 3723-3728.
- Z. S. Wu, Y. Sun, Y. Z. Tan, S. Yang, X. Feng and K. Mullen, *J. Am. Chem. Soc.*, 2012, **134**, 19532-19535.
- Y. Tao, D. Kong, C. Zhang, W. Lv, M. Wang, B. Li, Z.-H. Huang, F. Kang and Q.-H. Yang, *Carbon*, 2014, **69**, 169-177.
- C. Cui, W. Qian, Y. Yu, C. Kong, B. Yu, L. Xiang and F. Wei, *J. Am. Chem. Soc.*, 2014, **136**, 2256-2259.
- X. Li, J. Damien, L. Jiayan, J. Hee Dong, H. Jiaying and H. Zhen, *J. Power Sources*, 2012, **208**, 187-192.
- Y. Xu, Z. Lin, X. Huang, Y. Wang, Y. Huang and X. Duan, *Adv. Mater.*, 2013, **25**, 5779-5784.
- Z. Wen, X. Wang, S. Mao, Z. Bo, H. Kim, S. Cui, G. Lu, X. Feng and J. Chen, *Adv. Mater.*, 2012, **24**, 5610-5616.
- J. Luo, H. D. Jang, T. Sun, L. Xiao, Z. He, A. P. Katsoulidis, M. G. Kanatzidis, J. M. Gibson and J. Huang, *ACS Nano*, 2011, **5**, 8943-8949.
- M. Beidaghi and Y. Gogotsi, *Energy & Envir. Sci.*, 2014, **7**, 867-884.
- M. Beidaghi, Z. Wang, L. Gu and C. Wang, *J. Solid State Electrochem.*, 2012, **16**, 3341-3348.
- X. Ma, M. R. Zachariah and C. D. Zangmeister, *Nano Lett.*, 2012, **12**, 486-489.
- Z. Niu, L. Zhang, L. Liu, B. Zhu, H. Dong and X. Chen, *Adv. Mater.*, 2013, **25**, 4035-4042.
- X. Yang, J. Zhu, L. Qiu and D. Li, *Adv. Mater.*, 2011, **23**, 2833-2838.

Journal Name

30. X. Wang, Y. Zhang, C. Zhi, X. Wang, D. Tang, Y. Xu, Q. Weng, X. Jiang, M. Mitome, D. Golberg and Y. Bando, *Nat. Commun.*, 2013, **4**, 2905.
31. H. Wang, X. Sun, Z. Liu and Z. Lei, *Nanoscale*, 2014, **6**, 6577-6584.
32. W. Lv, Z. Li, G. Zhou, J.-J. Shao, D. Kong, X. Zheng, B. Li, F. Li, F. Kang and Q.-H. Yang, *Adv. Funct. Mater.*, 2014, **24**, 3456-3463.
33. Z. Niu, J. Chen, H. H. Hng, J. Ma and X. Chen, *Adv. Mater.*, 2012, **24**, 4144-4150.
34. D. Teweldebrhan and A. A. Balandin, *Appl. Phys. Lett.*, 2009, **94**, 013101.
35. S. J. An, Y. Zhu, S. H. Lee, M. D. Stoller, T. Emilsson, S. Park, A. Velamakanni, J. An and R. S. Ruoff, *J. Phys. Chem. Lett.*, 2010, **1**, 1259-1263.
36. Y. Yoon, S. Seo, G. Kim and H. Lee, *Chem. -Eur. J.*, 2012, **18**, 13466-13472.
37. C. N. Rao, A. K. Sood, K. S. Subrahmanyam and A. Govindaraj, *Angew. Chem. Int. Ed.*, 2009, **48**, 7752-7777.
38. U. N. Maiti, J. Lim, K. E. Lee, W. J. Lee and S. O. Kim, *Adv. Mater.*, 2014, **26**, 615-619.
39. Y. Meng, K. Wang, Y. Zhang and Z. Wei, *Adv. Mater.*, 2013, **25**, 6985-6990.
40. Q. Cheng, J. Tang, J. Ma, H. Zhang, N. Shinya and L. C. Qin, *Phys. Chem. Chem. Phys.*, 2011, **13**, 17615-17624.
41. Q. Cheng, J. Tang, J. Ma, H. Zhang, N. Shinya and L.-C. Qin, *Carbon*, 2011, **49**, 2917-2925.
42. H. Wang, Z. Xu, A. Kohandehghan, Z. Li, K. Cui, X. Tan, T. J. Stephenson, C. K. King'ondeu, C. M. Holt and B. C. Olsen, *ACS nano*, 2013, **7**, 5131-5141.
43. M. F. El-Kady, V. Strong, S. Dubin and R. B. Kaner, *Science*, 2012, **335**, 1326-1330.